Fluid modeling of waves and turbulence in plasma with temperature anisotropy

P.L. Sulem

in collaboration with

T. Passot, D. Laveder, P. Hunana, D. Borgogno

Waves and Instabilities in Space and Astrophysical Plasmas
Eilat, Israel, June 19-24, 2011

OUTLINE

- Space plasmas: Main features and debated questions
- How to model collisionless plasmas ?
- FLR-Landau fluid simulations

Space plasmas: Main features and debated questions

Space plasmas are magnetized and turbulent

β parameter is usually close to or larger than unity
Sonic Mach number is of order unity

Fluctuations cover a huge range of scales,
displaying power-law spectra that extend down to the
ion gyroscales where kinetic effects cannot be ignored.

Presence of coherent structures

Among the debated questions:
- Spectral energy distribution and its anisotropy
- Dissipation mechanisms
- Heating of the plasma: temperature anisotropy
- Particle acceleration

The concepts of waves make sense even in the strong turbulence regime.
Dispersion is non negligible at the ion scales: coherent structures.

Main features of solar wind plasma

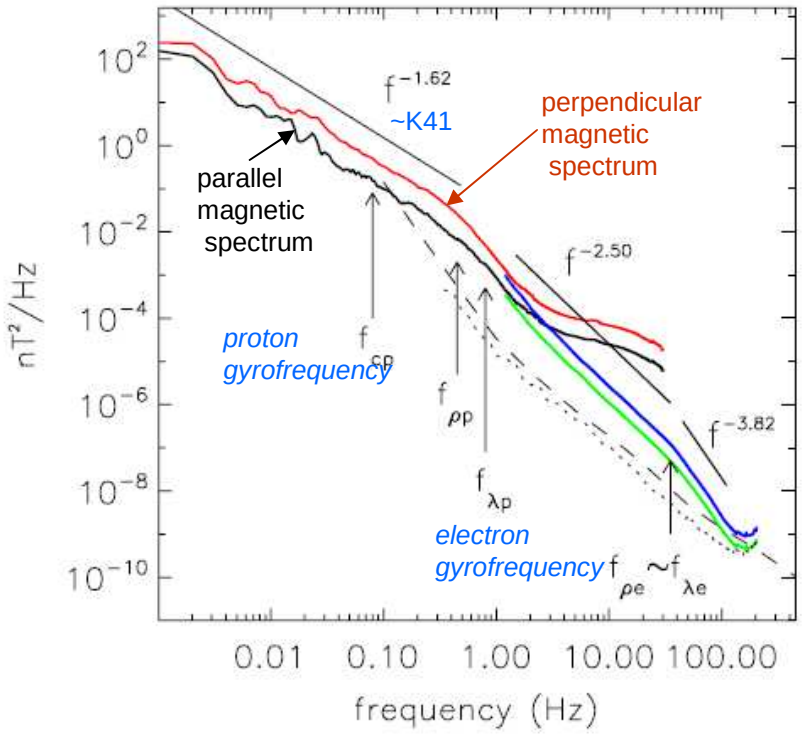

FIG. 2 (color online). The parallel (black) and perpendicular (red) magnetic spectra of FGM data ($f < 33$ Hz) and STAFF-SC data (respectively, light line; green online and dark line; blue online); $1.5 < f < 225$ Hz). The STAFF-SC noise level as measured in the laboratory and in-flight are plotted as dashed and dotted lines, respectively. The straight black lines are power law fits to the spectra. The arrows indicate characteristic frequencies defined in the text.

k-filtering -> **wave vectors are highly oblique relatively to the ambient field** (θ=86°)

Sahraoui et al. PRL 102, 231102 (2009)

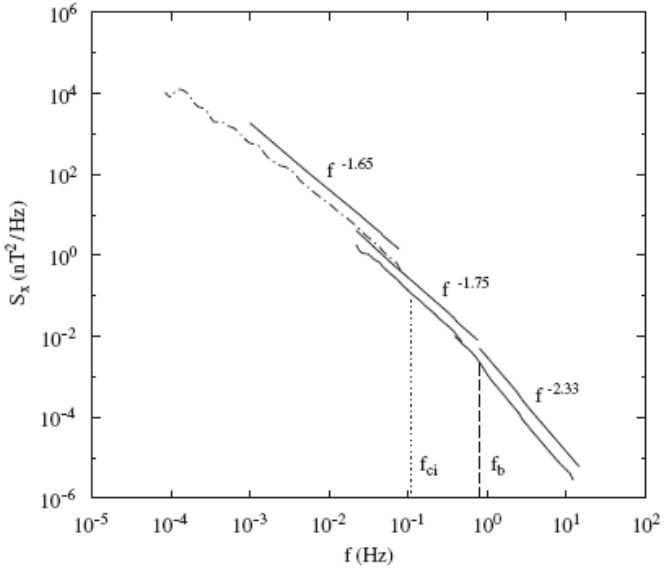

Energy spectra of B_x fluctuations measured by Cluster (full line) and by Helios 2 (dashed-dotted line)

Alexandrova et al. Planet. Space Sci. 55, 2224 (2007)

Excess of magnetic energy in the transverse components

Several power-law ranges:
Which waves? Which slopes?
Important to estimate the heating.
(*Ng et al. JGR 115, A02101, 2010*)

At what scales does dissipation take place?
By what mechanism?

Spectral anisotropy

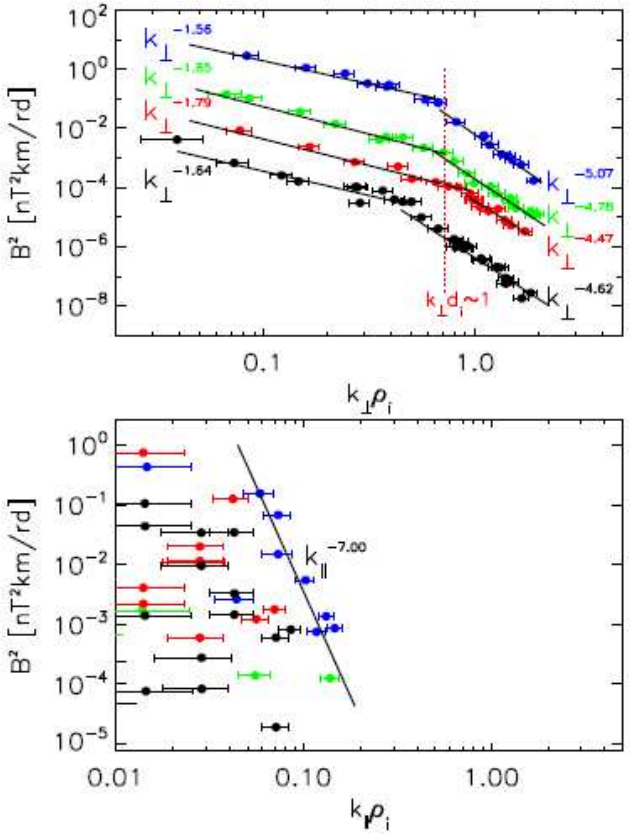

FIG. 6: Wave number spectra with estimated erro bars for the four time intervals in the parallel (bottom) and perpendicular (top) directions to the local mean field. The vertical dotted line shows the proton inertial length.

Quasi-transverse cascade
No power law in the parallel direction

Non resonnant heating of the protons, possibly via Landau damping

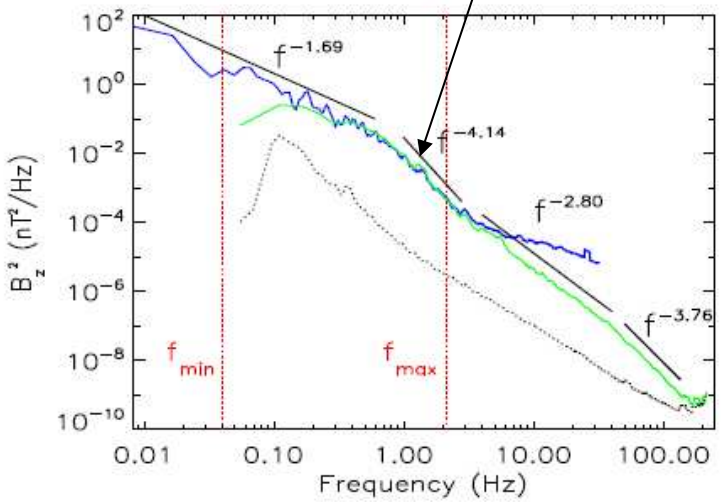

FIG. 3: B_z spectra measured by FGM (blue) and STAFF-SC (green) in DSI from 06:15 to 06:25 (flattening for $f \geq 3$ Hz is due to hitting the noise floor of the FGM). The black dotted line is the in-flight sensitivity floor of STAFF-SC.

Sahraoui et al. PRL 105, 131101 (2010)

Main features of terrestrial magnetosheath plasma

Important role of the temperature anisotropy: leads to micro-instabilities
AIC (near quasi-perpendicular shock) and mirror instabilities (further inside magnetosheath)

Presence of mirror modes

- Have essentially zero frequency in the plasma frame
- Identified using k-filtering technique
  (*Pinçon & Lefeuvre, JGR 96, 1789, 1991*).
- Spatial spectrum steeper than temporal one

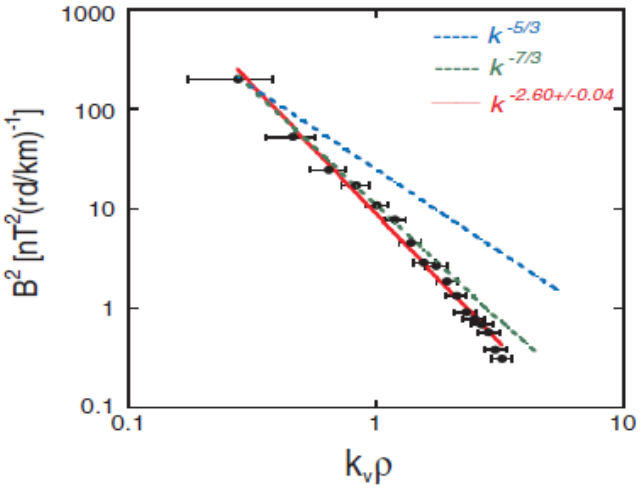

Sahraoui et al., PRL 96, 075002 (2006)

and of coherent structures:

- Current filaments and Alfvén vortices
- Mirror structures (magnetic holes and humps)

Drift kinetic Alfvén vortices also observed in the cusp region.
(*Sundkvist et al. Nature, 436, 825, 2005*)

Alfvén vortices

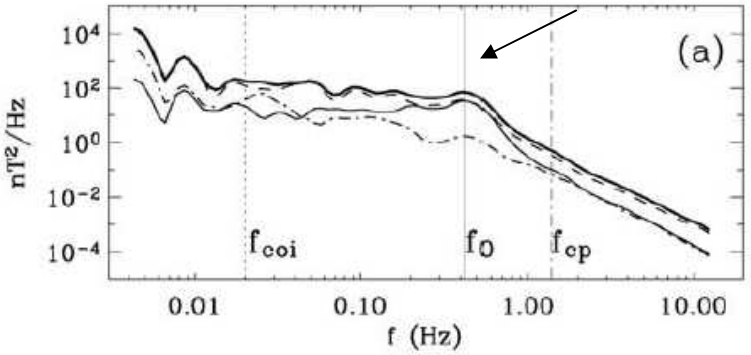

Alexandrova et al. JGR 111, A12208 (2006).

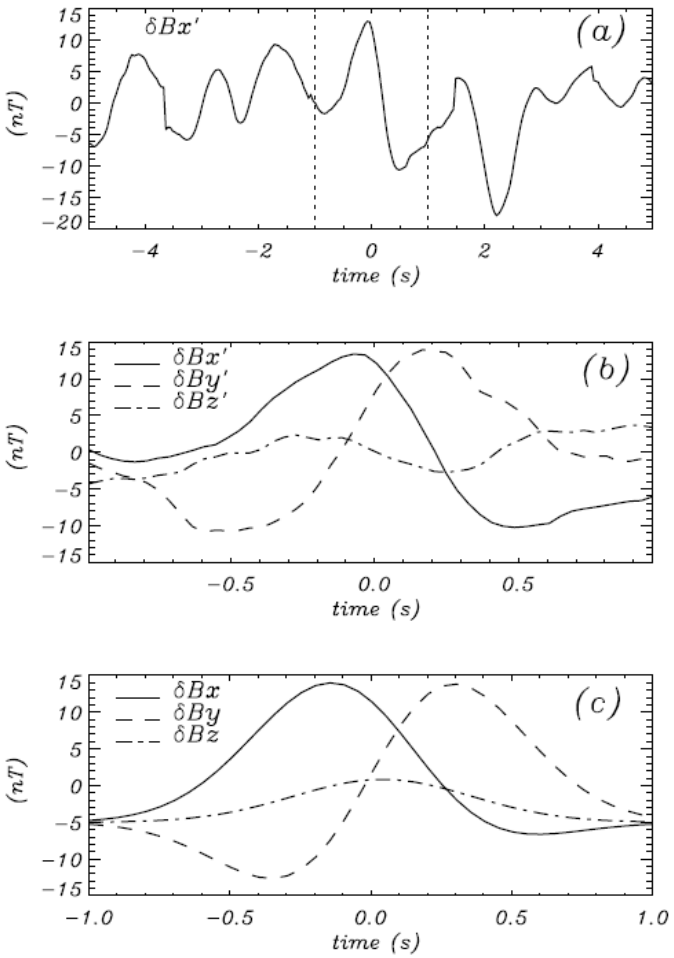

Figure 8. Magnetic field fluctuations, taking $\tau \simeq -420$ s (1755:16 UT) as the origin of time. (a) Fluctuations $\delta B_{x'}$ during 10 s around τ. (b) Fluctuations of the magnetic field components ($\delta B_{x'}$, $\delta B_{y'}$, $\delta B_{z'}$) for the 2-s period around τ. (c) The z-aligned current tube simulation (δB_x, δB_y, δB_z).

Signature of magnetic filaments
(Alexandrova et al. JGR 2004)

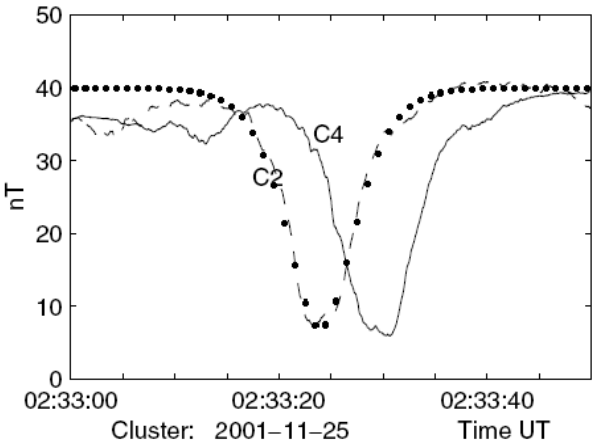

FIG. 1. A large scale soliton observed by Cluster spacecraft C2 (dashed) and C4 (solid) in the total magnetic field. Marked curve shows fit of $b_0\,\mathrm{sech}^2[(t-t_0)/\delta t]$ with $b_0 = -33$ nT and $\delta t = 4.4$ s. The soliton moves with velocity $u_0 \approx 250$ km/s and has a width of 2000 km. The position of Cluster satellites was $(-4, 17, 5)\ R_E$ GSE.

Slow magnetosonic solitons
(Stasiewicz et al. PRL 2003)

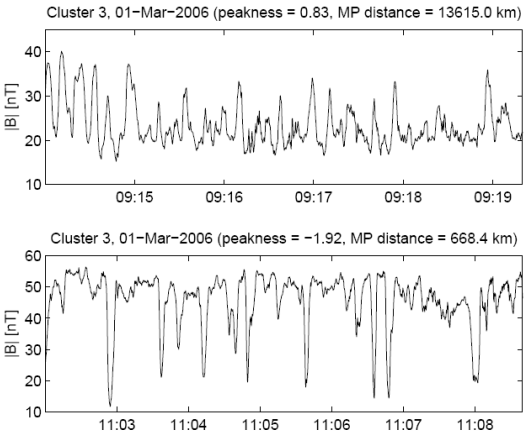

Mirror structures in the terrestrial magnetosheath
(Soucek et al. JGR 2008)

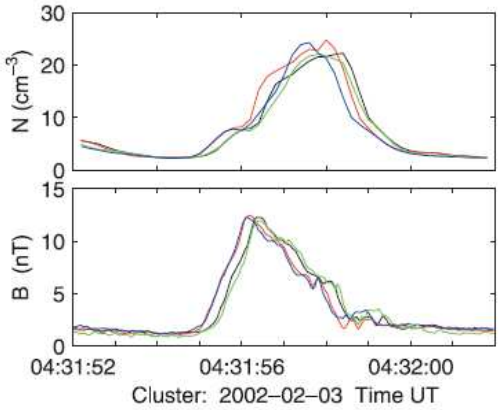

Figure 2. Pulse-like enhancements of the plasma density and magnetic field measured on four Cluster spacecraft: C1–C4, which are color coded in sequence: black, red, green, blue. The measurements represent signatures of fast magnetosonic shocklets moving with supersonic speed in a high-β plasma.

fast magnetosonic shocklets
(Stasiewicz et al. GRL 2003)

Statistical study of temperature anisotropies in the solar wind

Turbulence (and/or solar wind expansion) can generate temparature anisotropy
This anisotropy is constrained by micro-instabilities (mirror and oblique firehose) .

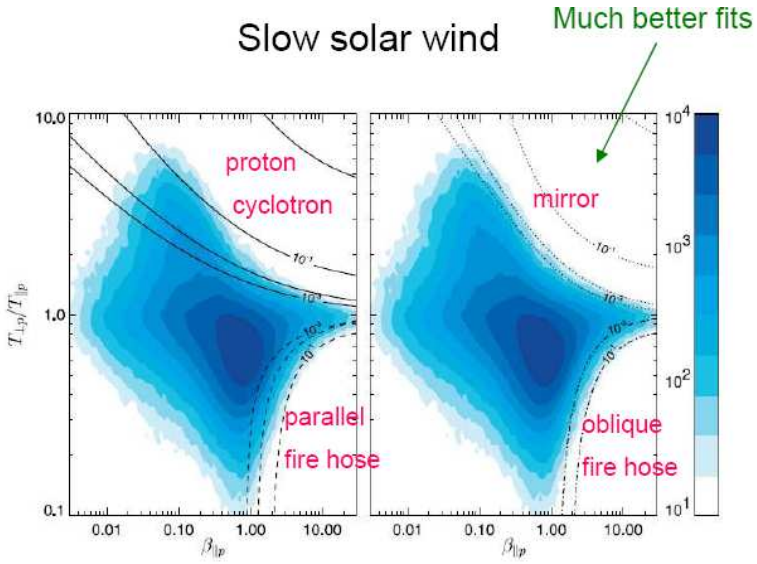

Figure 1. A color scale plot of the relative frequency of ($\beta_{\parallel p}$, $T_{\perp p}/T_{\parallel p}$) in the WIND/SWE data (1995–2001) for the solar wind with $v_{sw} \leq 600$ km/s [cf. *Kasper et al.*, 2002, Figure 2]. The (logarithmic) color scale is show on the right. The over plotted curves show the contours of the maximum growth rate (in units of ω_{cp}) in the corresponding bi-Maxwellian plasma (left) for the proton cyclotron instability (solid curves) and the parallel fire hose (dashed curves) and (right) for the mirror instability (dotted curves) and the oblique fire hose (dash-dotted curves).

*Hellinger et al. GRL **33**, L09101 (2006)*

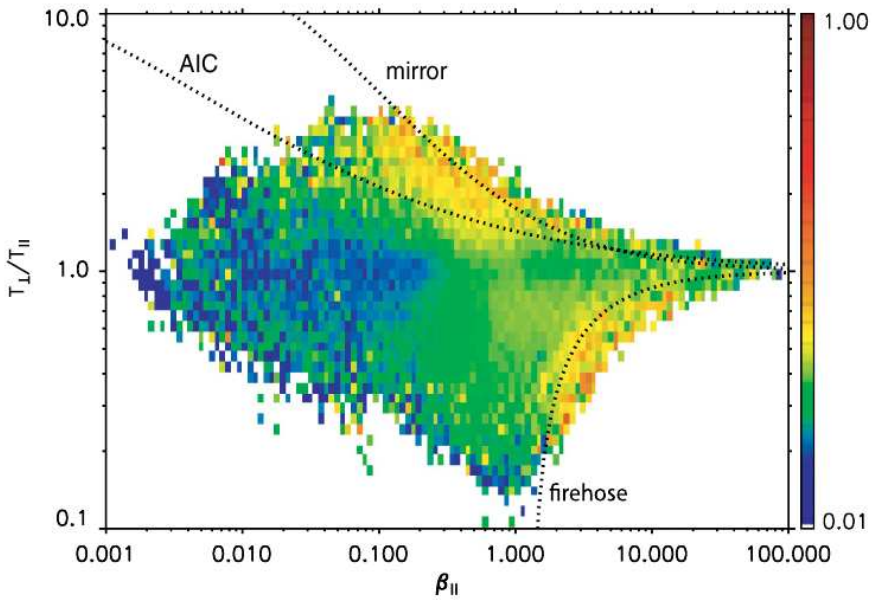

*Bale et al. PRL **103**, 21101 (2009)*

How to model collisionless plasmas ?

The solar wind is only very weakly collisional: this suggests kinetic simulations

Vlasov-Maxwell simulations: hardly possible on the present day computers in three space dimensions *(6 variables + time, and **a broad range of time scales**).*

Gyrokinetic simulations (*G. Howes, PoP **15**, 055904 , 2008)* are now feasible and show the presence of cascades both in the physical and velocity spaces in the range $k_\perp \rho \geq 1$.

Gyrokinetic theory (*Howes, ApJ **651**, 2006, Schekochihin et al., ApJ Supp., **182**, 310, 2009),* concentrates on the quasi-transverse dynamics and averages out the fast waves.

Applicability to space plasmas of the gyrokinetic theory is still to be validated.

Gyrokinetic simulations remain challenging numerically and difficult to interpret.

One needs a fluid model that (even if not rigorously justified)
- can be integrated relatively fast,
- allows for strong temperature anisotropies
- does not a priori order out the fast magnetosonic waves.

Fluid approaches: The MHD and its extensions

Simplest approach: the incompressible MHD

Provides a reasonable description at scales large compared to plasma microscales

- Only one type of waves : Alfvén waves.
- Interaction between counter-propagative Alfvén waves
- Clear concept of cascades (for the Elsasser variables) both in the context of weak and strong turbulence.
- Balance or unbalance regime depending on equal or unequal energy fluxes associated with Alfvén waves modes propagating along the ambient magnetic field.
- Possibility to develop a phenomenology close to K41 (in spite of less universality)
- Relatively simple equations, which permits high-resolution simulations

Observational evidence of small density fluctuations

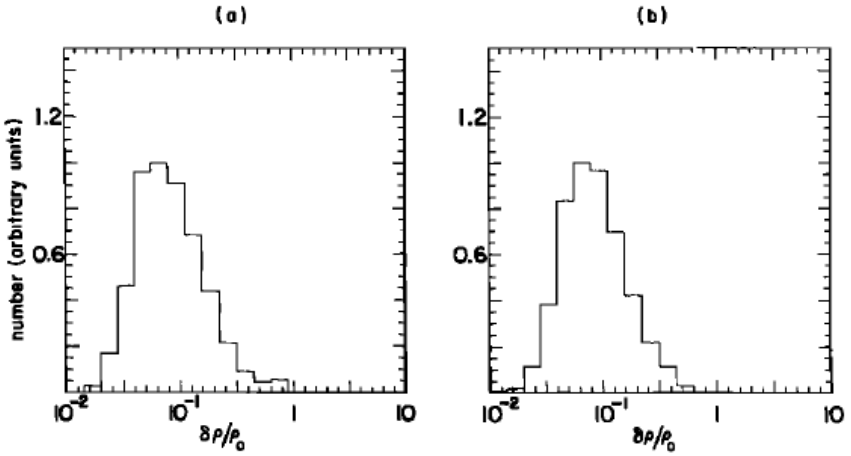

Fig. 2. Distribution of $\delta\rho/\rho_0$ for 7300 2-hour intervals of Voyager 2 data. (*a*) Data taken from radial distances of less than 5 AU. (*b*) Data taken between 5 and 10 AU. Here, $\delta\rho$ is computed from the rms of ρ over each 2-hour interval. Note that $\delta\rho/\rho_0$ is scaled logarithmically.

Matthaeus et al. JGR 1991

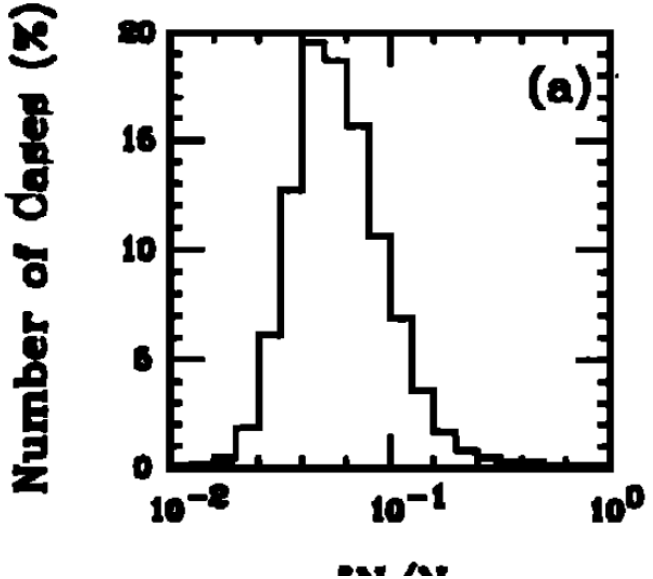

Histograms of (a) relative density fluctuations

Bavassano & Bruno, JGR 1995

Compressibility cannot be totally neglected

For incompressible homogeneous isotropic MHD turbulence, there exists of an analogous to the 4/5 law of Karman-Howarth for fluid turbulence, giving statistics of 3rd order moments for velocity increments

Elsässer variables: $\mathbf{z}^{\pm} = \mathbf{v} \pm \mathbf{b}$

$$\langle (z_L^-(\mathbf{x}+\mathbf{r}) - z_L(\mathbf{x}))|\mathbf{z}^+(\mathbf{x}+\mathbf{r}) - \mathbf{z}^+(\mathbf{x})|^2 \rangle = -\frac{4}{3}\epsilon^+ r$$

$$\langle (z_L^+(\mathbf{x}+\mathbf{r}) - z_L(\mathbf{x}))|\mathbf{z}^-(\mathbf{x}+\mathbf{r}) - \mathbf{z}^-(\mathbf{x})|^2 \rangle = -\frac{4}{3}\epsilon^- r$$

Longitudinal components

(*Politano & Pouquet, GRL **25**, 273, 1998*).

Compressibility is relevant even at large scales

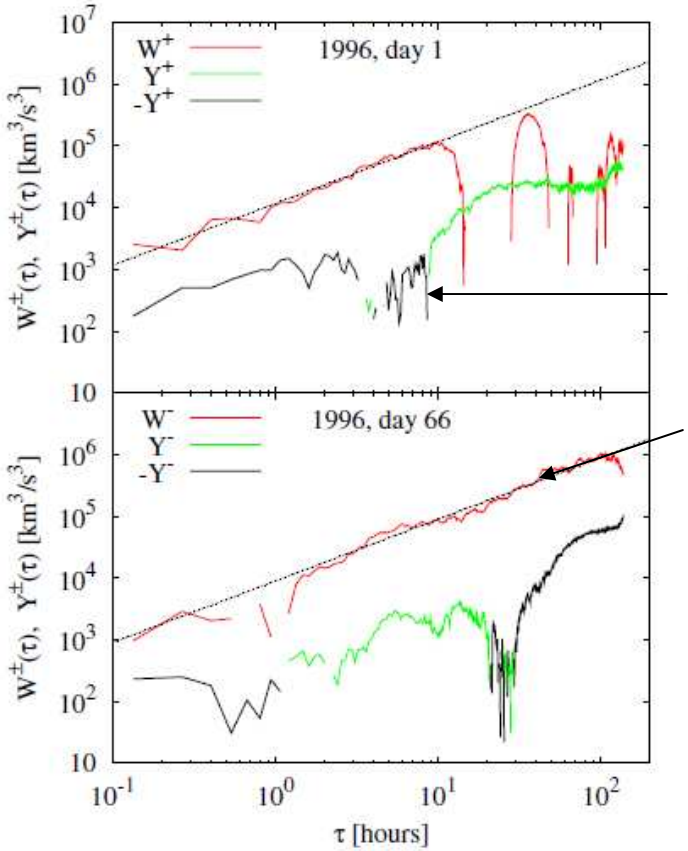

FIG. 2 (color online). Top panel: An example of the third-order compressible pseudoenergy flux $W^+(\tau)$ during days 1–10 of 1996. Bottom panel: $W^-(\tau)$ for days 66–75 of the same year. In both panels, the corresponding incompressible fluxes $Y^\pm(\tau)$ (no scaling present) and a linear fit are displayed.

Take compressibility into account in a phenomenological way:

$$Y^\pm(\ell) \equiv \langle |\Delta \mathbf{z}^\pm|^2 \Delta z_\parallel^\mp \rangle$$

$$\mathbf{w}^\pm \equiv \rho^{1/3} \mathbf{z}^\pm$$

$$W^\pm(\ell) \equiv \langle |\Delta \mathbf{w}^\pm|^2 \Delta w_\parallel^\mp \rangle \langle \rho \rangle^{-1} = -\tfrac{4}{3}\epsilon^\pm \ell$$

Significant effect despite small density fluctuations.

Carbone et al. PRL ***103,*** *061102 (2009)*

Compressible MHD retains waves that are damped by Landau resonance in Vlasov-Maxwell description of collisionless plasmas *(Howes, NPG 16, 219, 2009)*

MHD overestimates compressibility and energy transfer along the ambient field.

*Servidio et al. (PSS **55**, 2239, 2007):*
at ionic scales, spontaneous generation of quasi-perpendicular MS waves :
magnetosonic turbulence
(anti-correlation density magnetic intensity).

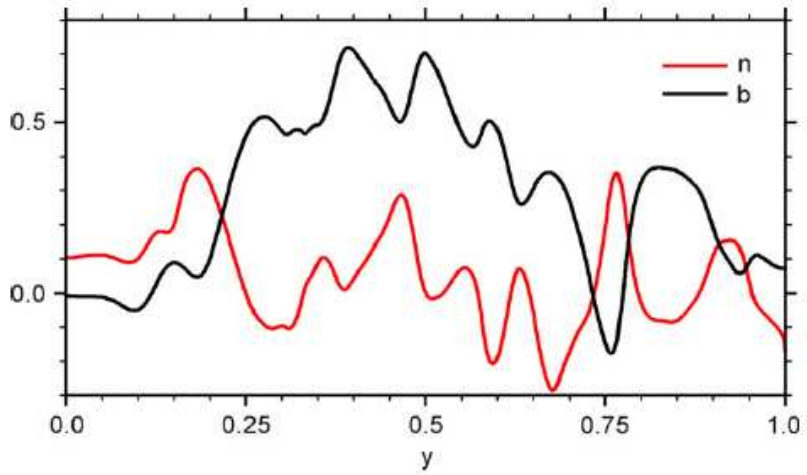

Fig. 3. The profile of fluctuating density δn (red line) and magnetic intensity δB (black line) obtained performing a cut along y-direction for $x = 0.5$ and $t = 18\tau_A$.

Contrasts with solar wind observations:
turbulence of quasi-transverse (kinetic) Alfvén waves
*(Sahraoui et al. PRL **105**, 131101, 2010).*

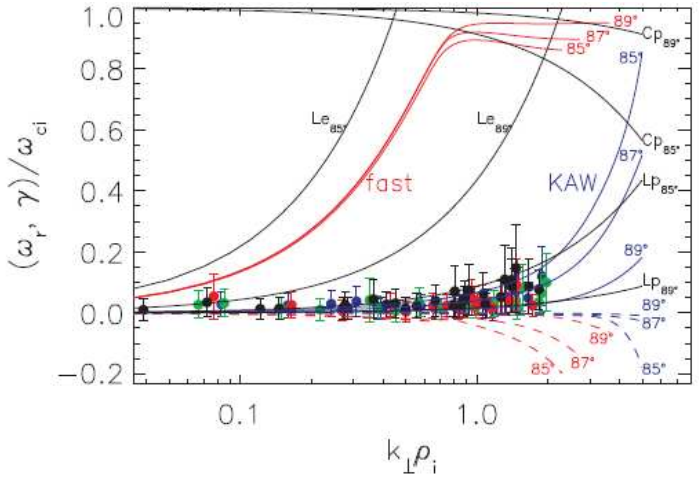

FIG. 5: Observed dispersion relations (dots), with estimated error bars, compared to linear solutions of the Maxwell-Vlasov equations for three observed angles Θ_{kB} (the dashed lines are the damping rates). The black curves ($L_{p,e}$) are the proton and electron Landau resonances $\omega = k_\parallel V_{th_{i,e}}$, the curves C_p are the proton cyclotron resonance $\omega = \omega_{ci} - k_\parallel V_{th_i}$ (the electron cyclotron resonance is also plotted but it lies expectedly out of the plotted frequency range).

Table 1. Mean Values of Plasma and Magnetic Field Data in the Analyzed Time Intervals: Characteristic Tetrahedron Size of Cluster L, Flow Speed V, Ion Number Density n, Magnitude of Magnetic Field B, Ion Temperature T, Plasma Parameter Beta (for Ions)

	L (km)	V (km/s)	n (cm^{-3})	B (nT)	T (MK)	Beta (1)
Interval 1	10,000	436.11	6.76	10.74	0.36	0.73
Interval 2	1000	446.26	3.35	7.59	0.28	0.57
Interval 3	100	443.05	6.69	10.13	0.32	0.72

Identification of a clear dispersion relation is difficult in spite of small fluctuation amplitudes and quasi-perpendicular propagation to the local mean magnetic field.

Frequency-wave number diagram exhibits largely scattered populations with only weak agreement with magnetosonic and whistler waves. Clear identification of a specific normal mode is difficult, suggesting that nonlinear energy cascade is operating even on small-scale fluctuations.

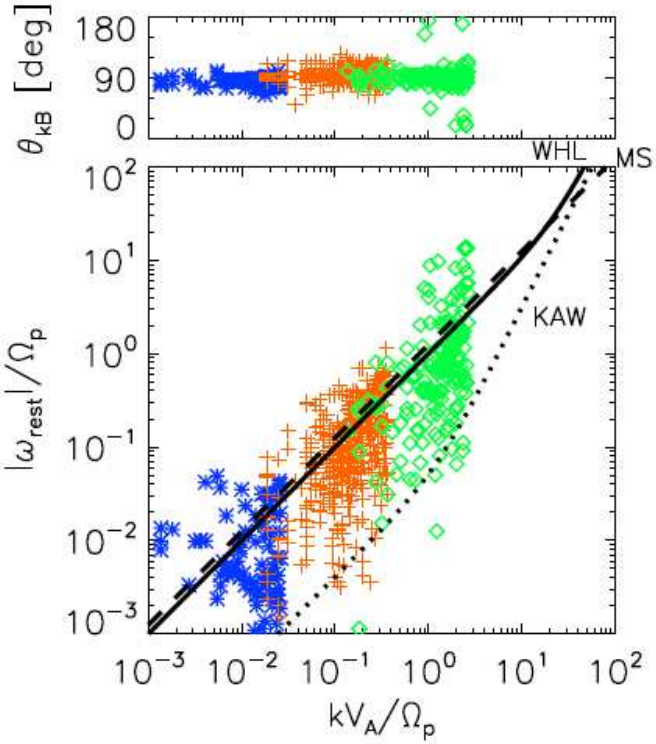

Figure 3. (top) Angles between the wave vectors and the mean magnetic field as a function of the wave number. (bottom) Frequency-wave number diagram of the identified waves in the plasma rest frame. Dashed, straight, and dotted lines represent dispersion relations for magnetosonic (MS), whistler (WHL), and kinetic Alfvén waves (KAW), respectively. Data from three intervals are integrated in the plots: left population with the asterisk symbols (in blue), middle with the plus symbols (in red), and right with the diamond symbols (in green) for Intervals 1, 2, and 3, respectively.

*Narita et al., GRL **38**, L05101(2011)*

Solar wind displays **temperature anisotropy**.

When the plasma is driven, temperature anisotropy can develop:
Beyond threshold, microinstabilities (i.e. the mirror instability) take place.

Mirror instability is driven by Landau damping, that is thus to be modelized.

For the problem to be linearly well-posed, instabilities should be arrested at small scales.
Finite Larmor corrections (non gyrotropic contributions) are to be retained to arrest the mirror instability at small scales.

It is necessary to retain

Landau damping

• to deplete sonic waves (and ensure a weaker compressibility)

• to correctly capture the mirror instability threshold

FLR corrections to arrest the mirror instability at small scales

These low-frequency kinetic effects should be included in a fluid approach
(in a way that does not induce spurious small-scale instabilities).

Gyrofluids: consists in closing the hierarchy of moment equations derived from the gyrokinetic equation.

Landau fluids: extension of anisotropic MHD including low-frequency kinetic effects: consistent with the linear kinetic theory, even at small transverse scales.

Fluid description retaining low-frequency kinetic effects: **Landau fluid models**

- Introduced by *Hammett & Perkins (PRL **64**, 3019, 1990)* as a closure retaining linear Landau damping.
- Applied to large-scale MHD by *Snyder, Hammett & Dorland (PoP **4**, 3974, 1997)* to close the hierarchy of moment equations derived from the drift kinetic equation.
- Extended to dispersive MHD with Hall effect and large scale FLR corrections *(Passot & Sulem, PoP **10**, 3906, 2003;Goswami, Passot & Sulem, PoP **12**, 102109, 2005)*
- Inclusion of quasi-transverse scales extending beyond the ion gyroscale, under the gyrokinetic scaling *(Passot & Sulem, PoP **14**, 082502, 2007)* : FLR-Landau fluids.

FLR-Landau fluids are based on a full description of the hydrodynamic nonlinearities, supplemented by a linear (or semi-linear) description of low-frequency kinetic effects (Landau damping and FLR corrections).

In contrast with gyrokinetics, Landau fluids retain fast waves that are accurately described up to the ion gyroscale.

Landau fluids (and also gyrofluids) neglect wave particle trapping, i.e. the effect of particle bounce motion on the distribution function near resonance.

Landau fluids

For the sake of simplicity, neglect electron inertia.

Ion dynamics: derived by computing velocity moments from Vlasov Maxwell equations.

$$\partial_t \rho_p + \nabla \cdot (\rho_p u_p) = 0$$

$$\partial_t u_p + u_p \cdot \nabla u_p + \frac{1}{\rho_p} \nabla \cdot \mathbf{p}_p - \frac{e}{m_p}(E + \frac{1}{c} u_p \times B) = 0$$

$$E = -\frac{1}{c}\left(u_p - \frac{j}{ne}\right) \times B - \frac{1}{ne} \nabla \cdot \mathbf{p}_e,$$

$$\partial_t B = -c \nabla \times E$$

$\rho_r = m_r n_r$

quasi-neutrality $(n_e = n_p)$

$$j = \frac{c}{4\pi} \nabla \times B$$

FLR corrections

$$\mathbf{p}_p = p_{\perp p} \mathbf{n} + p_{\parallel p} \boldsymbol{\tau} + \boldsymbol{\Pi}, \text{ with } \mathbf{n} = \mathbf{I} - \hat{b} \otimes \hat{b} \text{ and } \boldsymbol{\tau} = \hat{b} \otimes \hat{b}, \text{ where } \hat{b} = B / |B|.$$

Electron pressure tensor is taken gyrotropic
(considered scales >> electron Larmor radius)
and thus characterized by the parallel and transverse pressures $p_{\parallel e}$ and $p_{\perp e}$.

For each particle species,

heat flux tensor

Perpendicular and parallel pressures

$$\partial_t p_\perp + \nabla\cdot(u p_\perp) + p_\perp \nabla\cdot u - p_\perp \hat{b}\cdot\nabla u\cdot\hat{b} + \frac{1}{2}[\mathrm{tr}\,\nabla\cdot\mathbf{q} - \hat{b}\cdot(\nabla\cdot\mathbf{q})\cdot\hat{b}]$$
$$+\frac{1}{2}\left[\mathrm{tr}(\boldsymbol{\Pi}\cdot\nabla u)^S - (\boldsymbol{\Pi}\cdot\nabla u)^S{:}\boldsymbol{\tau} + \boldsymbol{\Pi}{:}\frac{d\boldsymbol{\tau}}{dt}\right] = 0$$

work of the nongyrotropic pressure force

$$\partial_t p_\parallel + \nabla\cdot(u p_\parallel) + 2p_\parallel \hat{b}\cdot\nabla u\cdot\hat{b} + \hat{b}\cdot(\nabla\cdot\mathbf{q})\cdot\hat{b} + (\boldsymbol{\Pi}\cdot\nabla u)^S{:}\boldsymbol{\tau} - \boldsymbol{\Pi}{:}\frac{d\boldsymbol{\tau}}{dt} = 0$$

Equations for the parallel and perpendicular (gyrotropic) heat fluxes

$$\partial_t q_\parallel + \nabla\cdot(q_\parallel u) + 3q_\parallel \hat{b}\cdot\nabla u\cdot\hat{b} + 3p_\parallel(\hat{b}\cdot\nabla)\left(\frac{p_\parallel}{\rho}\right) + \nabla\cdot(\tilde{r}_{\parallel\parallel}\hat{b}) - 3\tilde{r}_{\parallel\perp}\nabla\cdot\hat{b} + \partial_z R_\parallel^{NG} = 0$$

$$\partial_t q_\perp + \nabla\cdot(u q_\perp) + q_\perp\nabla\cdot u + p_\parallel(\hat{b}\cdot\nabla)\left(\frac{p_\perp}{\rho}\right) + \frac{p_\perp}{\rho}\left(\partial_x\Pi_{xz} + \partial_y\Pi_{yz}\right)$$
$$+\nabla\cdot(\tilde{r}_{\parallel\perp}\hat{b}) + \left((p_\parallel - p_\perp)\frac{p_\perp}{\rho} - \tilde{r}_{\perp\perp} + \tilde{r}_{\parallel\perp}\right)(\nabla\cdot\hat{b}) + \partial_z R_\perp^{NG} = 0$$

Involve the 4th-rank gyrotropic cumulants: $\tilde{r}_{\parallel\parallel}$, $\tilde{r}_{\parallel\perp}$, $\tilde{r}_{\perp\perp}$

$$\tilde{r}_{\parallel\parallel\parallel\parallel} = r_{\parallel\parallel\parallel\parallel} - 3\frac{p_\parallel^2}{\rho},$$

$$\tilde{r}_{\parallel\perp} = r_{\parallel\perp} - \frac{p_\perp p_\parallel}{\rho},$$

$R_\parallel^{NG}$ and $R_\perp^{NG}$ stand for the nongyrotropic contributions of the 4th-rank cumulants.

$$\tilde{r}_{\perp\perp} = r_{\perp\perp} - 2\frac{p_\perp^2}{\rho}.$$

Two main problems:

(1) Closure relations are needed to express the 4th-rank cumulants $\widetilde{r}_{\parallel\parallel}, \widetilde{r}_{\parallel\perp}, \widetilde{r}_{\perp\perp}$
(closure at lower or higher order also possible)

(2) (non gyrotropic) FLR corrections to the various moments are to be evaluated.

The starting point is the linear kinetic theory in the low-frequency limit:
Ω: ion gyrofrequency $\omega/\Omega \sim \epsilon \ll 1$

For a unified description of fluid and kinetic scales, FLR Landau-fluids retain contributions of:

- quasi-transverse fluctuations $(k_\parallel/k_\perp \sim \epsilon)$ with $k_\perp r_L \sim 1$
- hydrodynamic scales with $k_\parallel r_L \sim k_\perp r_L \sim \epsilon.$

r_L: ion Larmor radius

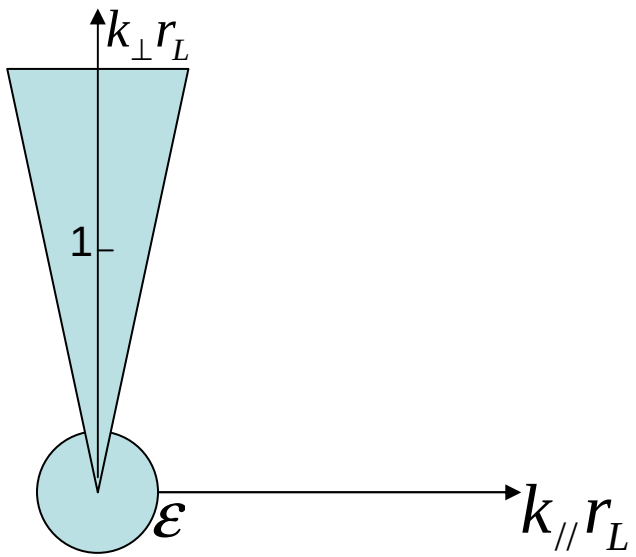

Brief description of the closure procedure

The closure is usually performed at the level of the 4th-rank moments
(model retaining full nonlinear dynamics of fourth order moments and closure at the level of fifth rank cumulants is in progress: aimed to a better description of departure from bi-Maxwellian regime).

The 4th-rank cumulants are obtained **from the linearized kinetic theory**,
assuming
small frequencies with respect to the ion gyrofrequency.
This requires
either long wavelengths with respect to the ion gyroradius
or
quasi-perpendicular directions.

The non-gyrotropic parts of the pressure, heat flux and 4th-rank tensors are also expressed using the kinetic theory.

IN PRACTICE:
*The above kinetic expressions typically depend on electromagnetic field components and involve the plasma dispersion function (which is nonlocal both in space and **time**).*

These various expressions can be expressed in terms of other fluid moments in such a way as to minimize the occurrence of the plasma dispersion function.

The latter is otherwise replaced by suitable Padé approximants, thus leading to local-in-time expressions. At some places, a Hilbert transform with respect to the longitudinal space coordinate appears, that modelizes Landau damping.

CLOSURE RELATIONS are based on linear kinetic theory (near bi-Maxwellian equilibrium) in the low-frequency limit.

For example, for each species, (assuming the ambient magnetic field along the z direction),

$$\widetilde{r}_{\parallel\perp} = \frac{{p_\perp^{(0)}}^2}{\rho^{(0)}} \left[1 - R(\zeta) + 2\zeta^2 R(\zeta)\right] \left[[2b\Gamma_0(b) - \Gamma_0(b) - 2b\Gamma_1(b)] \frac{b_z}{B_0} + b[\Gamma_0(b) - \Gamma_1(b)] \frac{e\Psi}{T_\perp^{(0)}} \right]$$

$\Gamma_n(b) = e^{-b} I_n(b)$, $b = (k_\perp^2 T_\perp^{(0)})/(\Omega^2 m)$, $I_n(b)$ modified Bessel function, $E_z = -\partial_z \Psi$

R is the plasma response function, $\zeta = \frac{\omega}{|k_\parallel| v_{th}}$. (For electrons, $b \approx 0$, $\Gamma_0 \approx 1$, $\Gamma_1 \approx 0$)

It turns out that $\widetilde{r}_{\parallel\perp}$ can be expressed in terms of perpendicular gyrotropic heat flux $q_\perp$ and of the parallel current j_z. One has

$$\widetilde{r}_{\parallel\perp} = \sqrt{\frac{2T_\parallel^{(0)}}{m}} \frac{1 - R(\zeta) + 2\zeta^2 R(\zeta)}{2\zeta R(\zeta)} \left[q_\perp + [\Gamma_0(b) - \Gamma_1(b)] \frac{p_\perp^{(0)} p_\parallel^{(0)}}{\rho^{(0)} v_A^2} \left(\frac{T_\perp^{(0)}}{T_\parallel^{(0)}} - 1 \right) \frac{j_z}{e n^{(0)}} \right]$$

The approximation consists in replacing the plasma response function R by the three pole Padé approximant $R_3(\zeta) = \dfrac{2 - i\sqrt{\pi}\zeta}{2 - 3i\sqrt{\pi}\zeta - 4\zeta^2 + 2i\sqrt{\pi}\zeta^3}$.

This leads to the approximation: $$\frac{1-R(\zeta)+2\zeta^2 R(\zeta)}{2\zeta R(\zeta)} \approx \frac{i\sqrt{\pi}}{-2+i\sqrt{\pi}\zeta}.$$

After substitution one gets an initial value problem:

Hilbert transform

$$\left(\frac{d}{dt} - 2|a_0|\sqrt{\frac{2T_\parallel^{(0)}}{m}}\mathcal{H}_z\partial_z\right)\tilde{r}_{\parallel\perp} + \frac{2T_\parallel^{(0)}}{m}\left(a_1 - \frac{1}{2}\right) \qquad a_0 = i/\sqrt{\pi},\ a_1 = 3/2$$

$$\times\partial_z\left[q_\perp + [\Gamma_0(b) - \Gamma_1(b)]\frac{p_\perp^{(0)}}{v_A^2}\left(\frac{T_\perp^{(0)} - T_\parallel^{(0)}}{m_p}\right)\frac{j_z}{en^{(0)}}\right] = 0.$$

In order to take into account the global evolution of the plasma, replace equilibrium quantities by instantaneous mean values.

Similarly, the gyroviscous tensor is computed by combining various fluid quantities obtained from the linear kinetic theory, allowing to eliminate most occurrences of the plasma dispersion function.

*Passot & Sulem, PoP **14**, 082502 (2007)*

Finite Larmor radius effects:

$$\overline{\overline{\Pi}}_\perp = \begin{pmatrix} \Pi_{xx} & \Pi_{xy} \\ \Pi_{yx} & \Pi_{yy} \end{pmatrix}$$

Gyroviscous tensor: $\overline{\overline{\Pi}} = \overline{\overline{\Pi}}_\perp + \Pi_\parallel \otimes \widehat{b} + \widehat{b} \otimes \Pi_\parallel$

$$\Pi_z = (\Pi_{xz}, \Pi_{yz}, \Pi_{zz})$$

It is convenient to write $\frac{1}{p_{\perp p}^{(0)}} \nabla_\perp \cdot \overline{\overline{\Pi}}_\perp = -\nabla_\perp \mathcal{A} + \nabla_\perp \times (\mathcal{B}\widehat{z})$.

By combining expressions of the various fields provided by the kinetic theory in order to eliminate the plasma response function, one gets

$$\mathcal{A} = \left[1 - \frac{\Gamma_1(b)}{b[\Gamma_0(b) - \Gamma_1(b)]} + \frac{\Gamma_1(b)}{\Gamma_0(b)}\right] \frac{1}{\Omega}(ik_\perp \times u_{\perp p}) \cdot \widehat{z} - \frac{\Gamma_1(b)}{\Gamma_0(b)} \frac{T_{\perp p}^{(1)}}{T_{\perp p}^{(0)}}$$

$$\mathcal{B} = -\left[\frac{\Gamma_0(b) - 1 - \Gamma_1(b)}{b} + 2(\Gamma_0(b) - \Gamma_1(b)) + \frac{\Gamma_0(b) - \Gamma_1(b)}{1 - \Gamma_0(b)}(\Gamma_0(b) - \Gamma_1(b) - \frac{1 - \Gamma_0(b)}{b})\right]$$

$$\times \frac{c}{\Omega B_0}(ik_\perp \times E_\perp) \cdot \widehat{z} + \frac{1}{1 - \Gamma_0(b)}\left[\Gamma_0(b) - \Gamma_1(b) - \frac{1 - \Gamma_0(b)}{b}\right] \frac{1}{\Omega}(ik_\perp \cdot u_{\perp p}).$$

In the large scale limit $b = \frac{k_\perp^2}{\Omega^2} \frac{T_{\perp p}^{(0)}}{m_p} \to 0$, the usual fluid estimates are recovered:

$$\mathcal{A}_{fluid} = \tfrac{1}{2\Omega}(\nabla_\perp \times u_\perp) \cdot \widehat{z}, \quad \mathcal{B}_{fluid} = \tfrac{1}{2\Omega}(\nabla_\perp \cdot u_\perp)$$

In order to reproduce the leading-order nonlinear fluid theory, replace $p_{\perp p}^{(0)}$ by $p_{\perp p}$

Similar analysis for $\Pi_z = (\Pi_{xz}, \Pi_{yz}, \Pi_{zz})$.

In order to take into account the global evolution of the plasma, replace equilibrium quantities by instantaneous mean values.

The model conserves the total energy:

$$E = \int \left[\frac{\rho u^2}{2} + \frac{b^2}{2} + \frac{\beta}{2} \left(p_{\perp i} + p_{\perp e} + \frac{1}{2} (p_{\parallel i} + p_{\parallel e}) \right) \right] d\xi$$

Conservation of energy is independent of the heat fluxes and subsequent equations, but requires retaining the work done by the FLR stress forces.

Implementation of the Landau damping via Hilbert transforms, and also of the FLR coefficients as Bessel functions of $k_\perp \rho$, is easy in a spectral code.

Electron Landau damping is an essential ingredient in many cases (limiting the range of validity of the isothermal models).

Possibility of including weak collisions (Gross and Krook 1956, Green 1973) in a form that preserve energy conservation.

Mirror modes growth rate: comparison of FLR-Landau fluid with kinetic theory

(WHAMP code)

Normalized growth rate ω_i/Ω_p versus $k_\perp r_L$

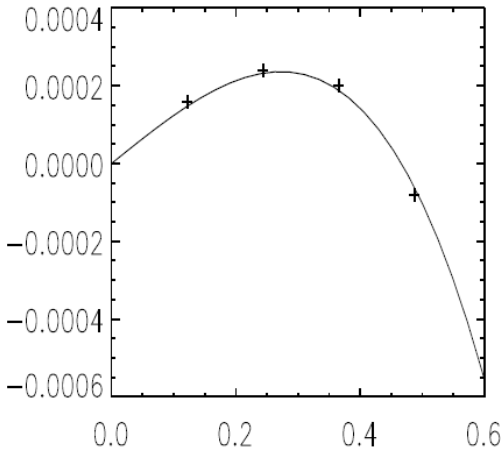

$\tau = T_{\|e}/T_{\|p}$

$\beta = 5,\ \tau = 0.1,\ \theta = \cos^{-1}(.1),$
$T_{\perp p}/T_{\|p} = 1.2$ and $T_{\perp e}/T_{\|e} = 1.$

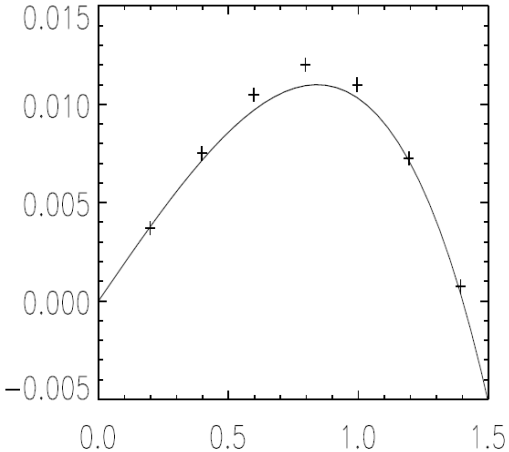

$\beta = 2,\ \tau = 1,\ \theta = \cos^{-1}(.1),$
$T_{\perp p}/T_{\|p} = 2$ and $T_{\perp e}/T_{\|e} = 1.$

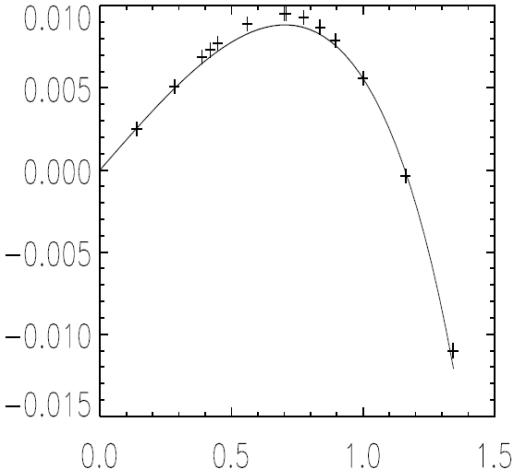

$T_{\perp p}/T_{\|p} = 1.4$ and $T_{\perp e}/T_{\|e} = 1.$

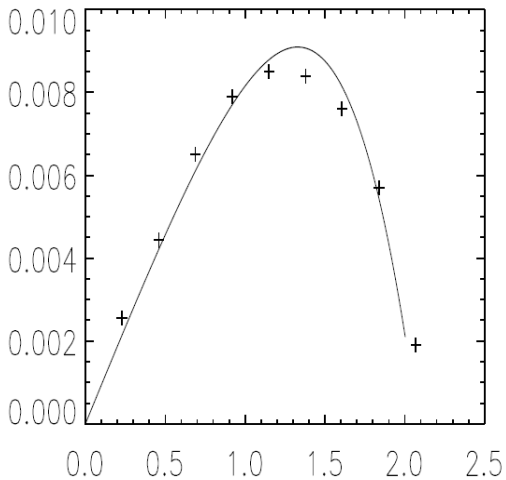

$T_{\perp p}/T_{\|p} = 1.1$ and $T_{\perp e}/T_{\|e} = 1.18$

$\beta = 5,\ \tau = 1,\ \theta = \cos^{-1}(.2),$

Frequency and damping rate of Alfvén waves:

quasi-transverse propagation (Kinetic Alfvén waves)

frequency damping rate

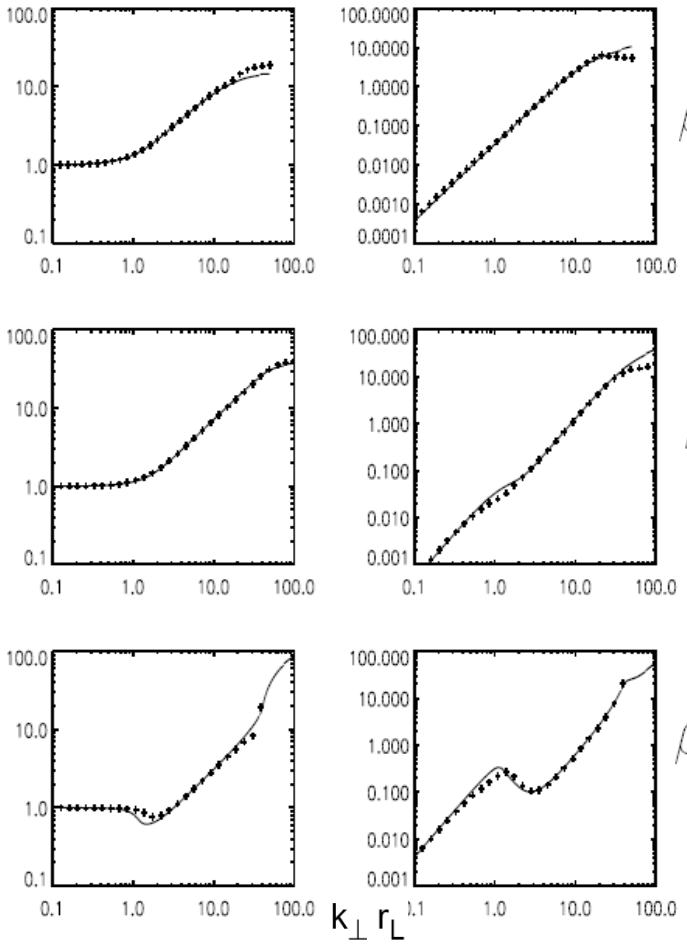

FIG. 2: Normalized frequency $\omega_r/(k_\parallel v_A)$ (left) and damping rate $-\omega_i/(k_\parallel v_A)$ (right) for KAWs with $\theta = \tan^{-1}(1000)$, $\tau = 1$, versus $k_\perp r_L$ for $\beta = 0.1$ (top), $\beta = 1$ (middle), $\beta = 10$ (bottom).

θ=89.9°

Does not capture resonance

oblique propagation

θ≈84° $\theta = \tan^{-1}(10)$

frequency damping rate

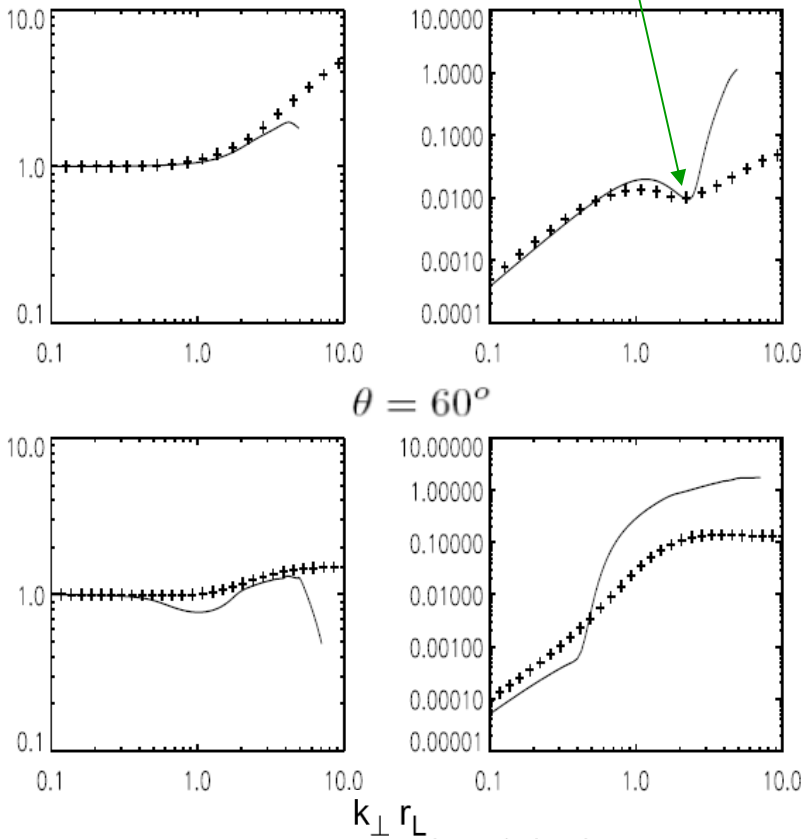

FIG. 3: Normalized frequency $\omega_r/(k_\parallel v_A)$ (left) and damping rate $-\omega_i/(k_\parallel v_A)$ (right) for KAWs with $\tau = 0.01$, $\beta = 1$ versus $k_\perp r_L$ for $\theta = \tan^{-1}(10)$ (top), $\theta = 60^o$ (bottom).

Nonlinear regime

Numerical simulations in one-space dimension:
talk by T. Passot

A 3D code is presently under development
(some simplifications seem possible and are under test)

In some instances,the model can simplify by taking the large scale limit

One gets (in the local reference frame):

Heat flux contribution requires special attention as it may in some instances lead to spurious instabilitites in oversimplified models.

$$\Pi_{xx} = -\Pi_{yy} = -\frac{\langle p_\perp \rangle}{2\Omega_i}(\partial_y u_x + \partial_x u_y),$$

$$\Pi_{xy} = \Pi_{yx} = -\frac{\langle p_\perp \rangle}{2\Omega_i}(\partial_y u_y - \partial_x u_x),$$

$$\Pi_{yz} = \Pi_{zy} = \frac{1}{\Omega_i}\left[2\langle p_\parallel \rangle \partial_z u_x + \langle p_\perp \rangle(\partial_x u_z - \partial_z u_x) + \partial_x q_\perp\right]$$

$$\Pi_{xz} = \Pi_{zx} = -\frac{1}{\Omega_i}\left[2\langle p_\parallel \rangle \partial_z u_y + \langle p_\perp \rangle(\partial_y u_z - \partial_z u_y) + \partial_y q_\perp\right]$$

$$\Pi_{zz} = 0.$$

The inclusion of FLRs in the MHD equations is considered in many models aiming to modelize the slow or drift dynamics in fusion plasmas.

The above simplified FLR can be inappropriate in the presence of temperature anisotropy:

When using the above simplified FLR's, the mirror instability is stabilized only very close to threshold and spurious instabilities can develop at smaller scales.

(the functions Γ_0 and Γ_1 are to be retained).

large-scale model

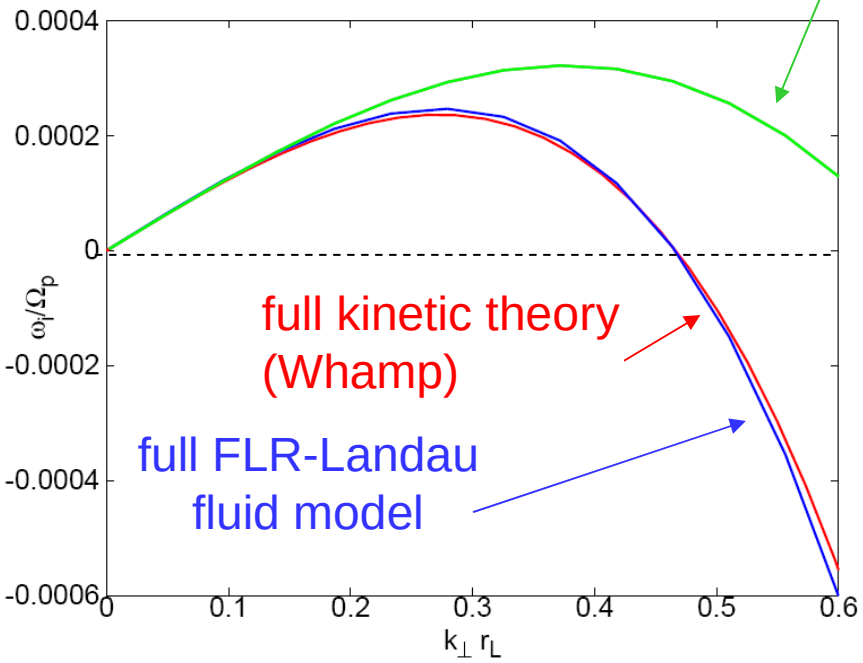

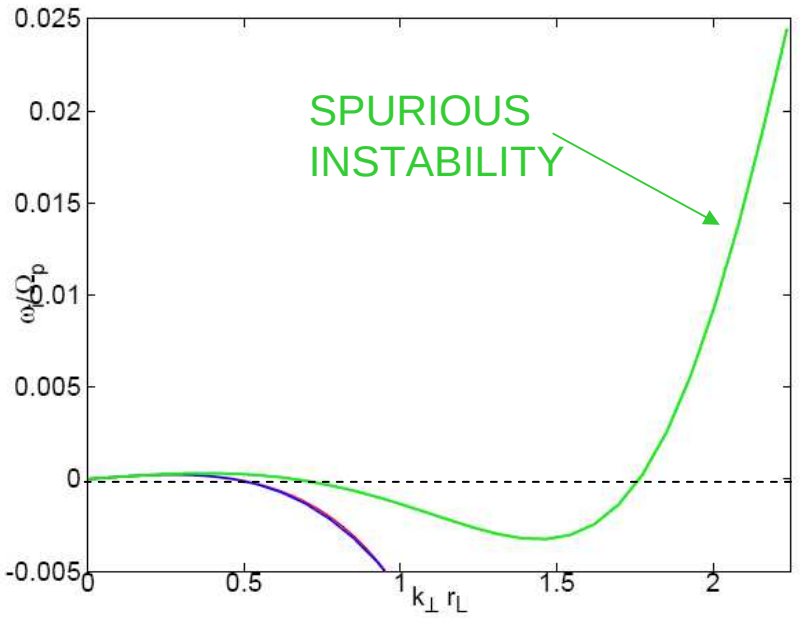

$$\tau = T_{\|e}/T_{\|p}$$

$$\beta = 5,\ \tau = 0.1,\ \theta = \cos^{-1}(.1) \text{ =84.26°}$$
$$T_{\perp p}/T_{\|p} = 1.2 \text{ and } T_{\perp e}/T_{\|e} = 1.$$

expansion parameter ε=0.1

Electron FLR corrections and electron inertia neglected in the FLR Landau fluid

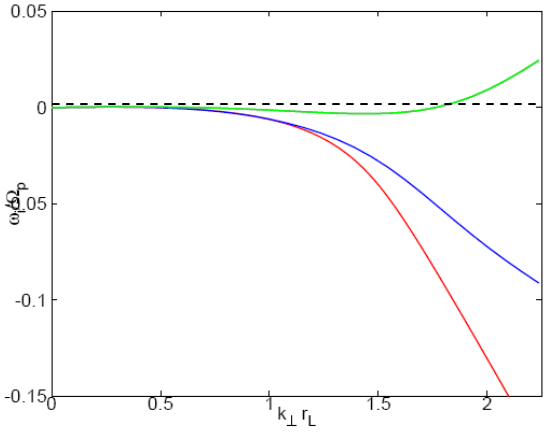

Examples of use of the simplified FLR Landau fluid

Decay instability of parallel Alfvén waves in the long-wavelength limit

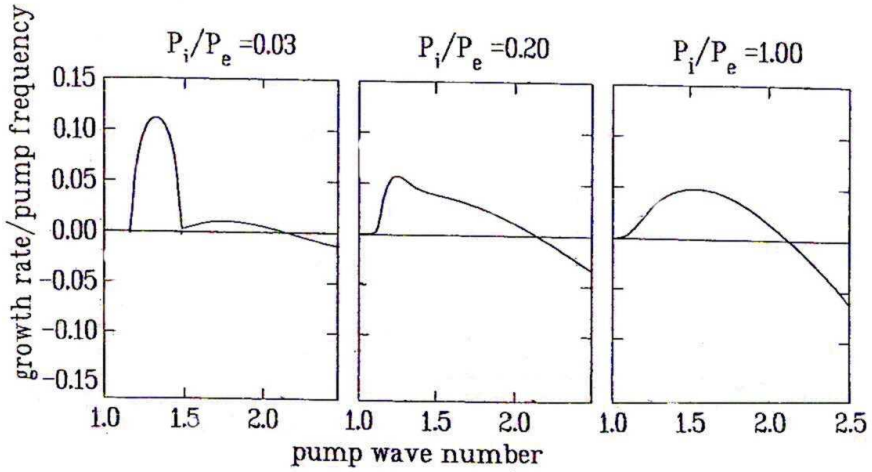

Drift-kinetic analysis (from Inhester 1990)

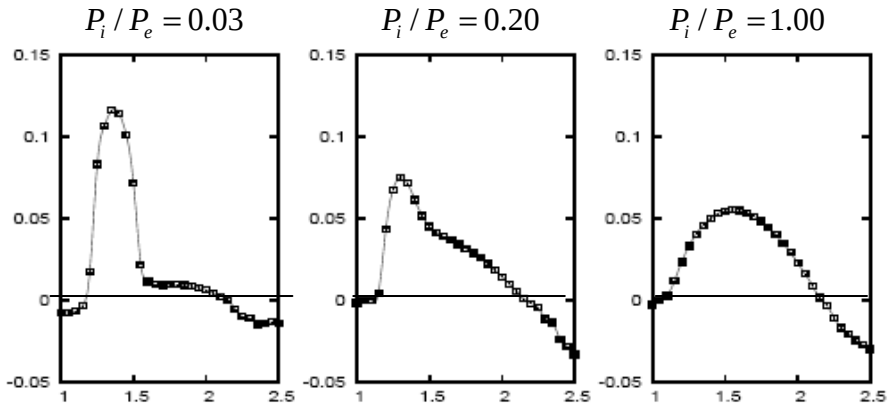

Landau fluid simulation

Maximum growth rates of the density modes versus wavenumber (normalized by the pump wavenumber) resulting from the decay instability of a non dispersive Alfvén wave of amplitude $b_0 = 0.447$ in a plasma with $\beta_{\|p} = 0.3$ and isotropic temperatures such that $T_e^{(0)}/T_p^{(0)} = 33$ (left), $T_e^{(0)}/T_p^{(0)} = 5$ (middle) and $T_e^{(0)}/T_p^{(0)} = 1$ (right).

Reducing electron temperature tends to broaden the spectral range and to reduce the growth rate of the instability.

Decay instability of Alfvén wave produces a forward propagating acoustic wave and a backward Alfvén wave with a wavenumber smaller than that of the pump.

Nonlinear simulations:

- A three-dimensional parallel code was developed for the simplified FLR-Landau fluid

Comparison between Landau fluid and hybrid PIC simulations

Propagation of an Alfvén wave in a density inhomogeneity: parallel high density channel of small amplitude (10%), aligned with the ambient field

Landau fluid PIC

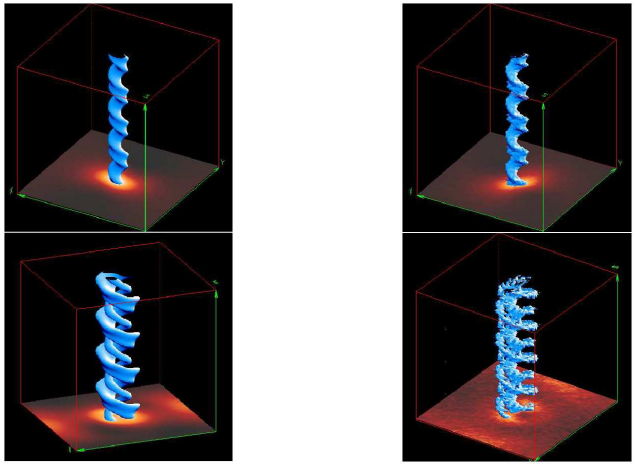

$T_e / T_p = 1/30$

$\beta_p = 0.3 \quad \beta_e = 0.01$

*(Borgogno et al. NPG **16**, 275, 2009)*

Density hump of large amplitude (100%)

Early formation of magnetic filament is followed by the onset of thin helical ribbons

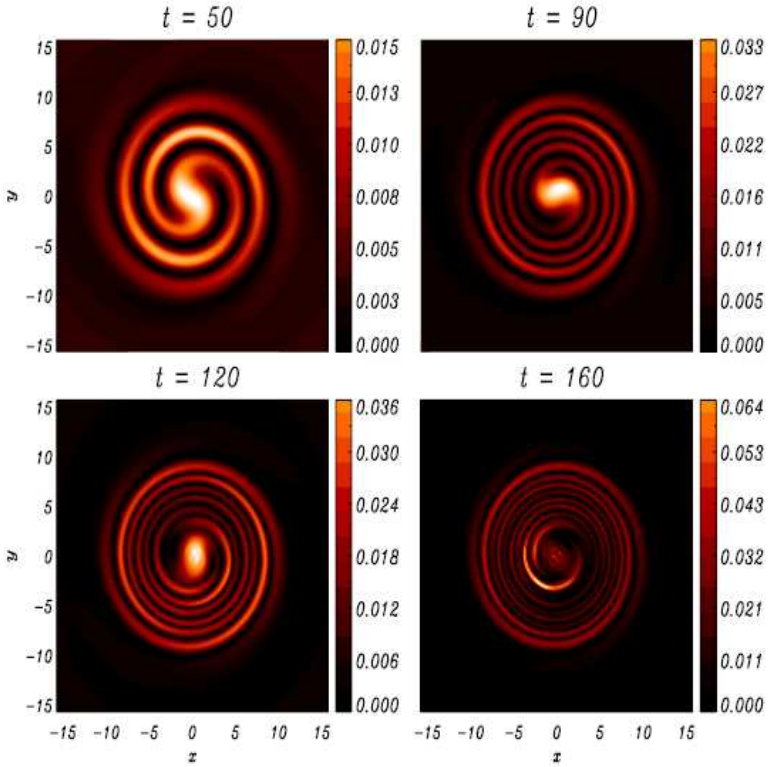

Cross section

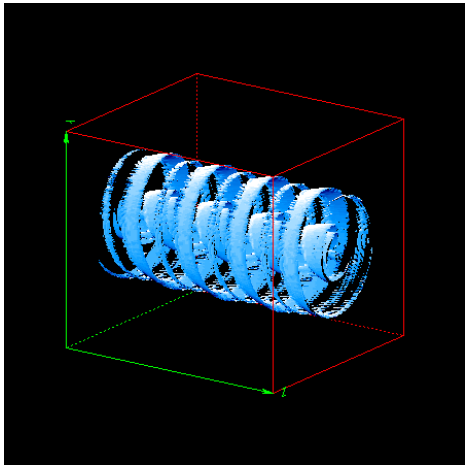

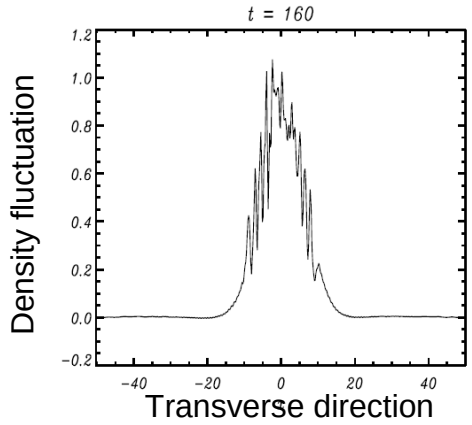

Borgogno et al. NPG 16, 275 (2009)

Developement of strong gradients and of scales smaller than the ion Larmor radius.
The spatial support of small-scale structures is more extended than without dispersion
(small-scales concentrated on localized oblique shocks).
"Dispersive phase mixing": **importance of 3D geometry** and of ion Landau damping

This suggests to **perform 3D PIC simulations** similar to the 2D simulations of *Tsiklauri et al.2005, Mottez et al. 2006.*

3D FLR-Landau fluid simulations in a turbulent regime

(simplified model) *Hunana et al., submitted to ApJ*

Freely decaying turbulence (temperatures remain close to their initial values)

Isothermal electrons
Initially, no temperature anisotropy; equal ion and electron temperatures
Incompressible initial velocity.

Pseudo-spectral code
Resolution: 128^3 (with small scale filtering)

Size of the computational domain: 32 π inertial lengths in each direction
Initially, energy on the first 4 velocity and magnetic Fourier modes $kd_i = m/16$ (m=1,…,4) with flat spectra and random phase.

initial fluctuations: $\langle \boldsymbol{u}^2 \rangle^{1/2} = \langle \boldsymbol{b}^2 \rangle^{1/2} = 1/8$

ion pressures: $p_\perp = p_\parallel = 1$

density: $\rho = 1$

ion fluxes: $q_\perp = q_\parallel = 0$

electron temperature: $T_e^{(0)} = 1$

ambient field: $B_0 = 1$

Compressibility reduction

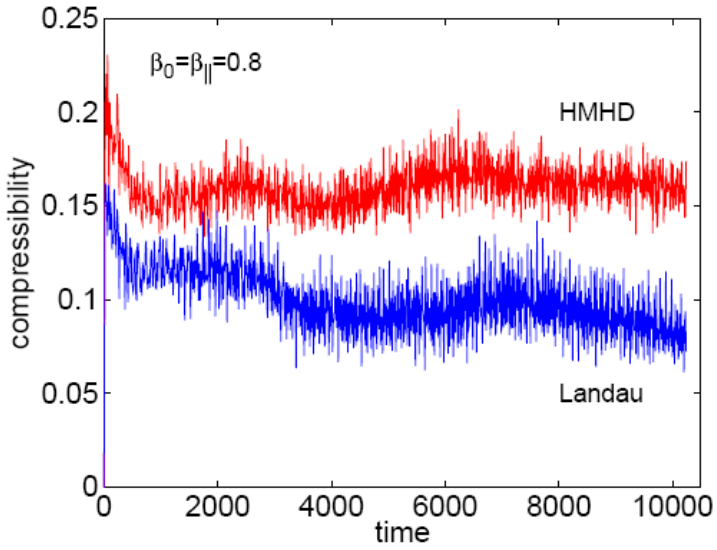

FIG. 6: Compressibility for Hall-MHD (red line) and FLR-Landau fluid (blue line) evaluated as $(\sum_k |\boldsymbol{k}\cdot\boldsymbol{u}_k|^2/|\boldsymbol{k}|^2)/\sum_k |\boldsymbol{u}_k|^2$ for $\beta_0 = \beta_{||} = 0.8$. Both regimes start with the identical initial condition where the velocity field is divergence free. The figure shows that the compressibility is clearly inhibited in the Landau fluid simulation.

Identification of the MHD modes (frequency analysis)

Hall-MHD FLR-Landau fluid

Left and right polarized Alfvén waves for the propagation angle of 0°

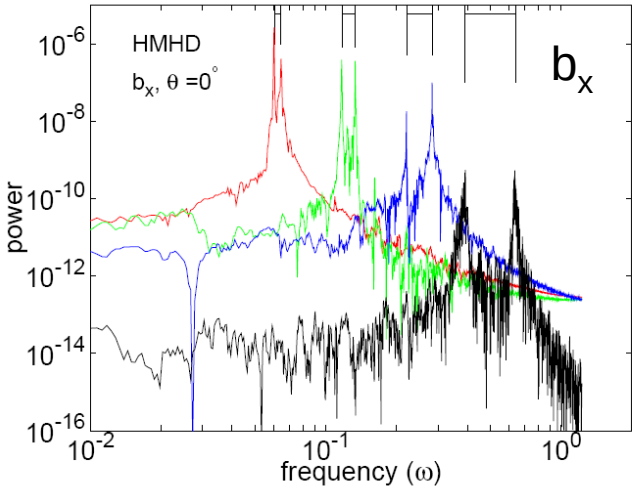

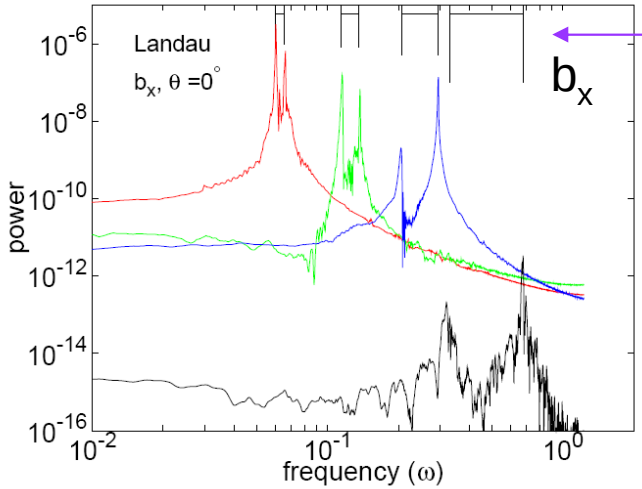

Prediction from dispersion relation

Sound waves for the propagation angle of 0°

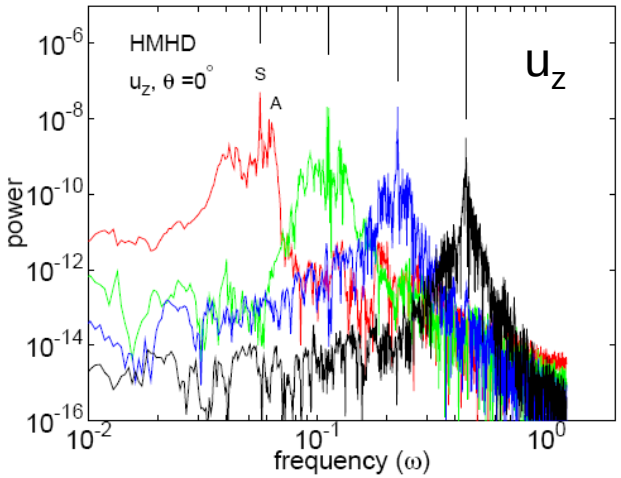

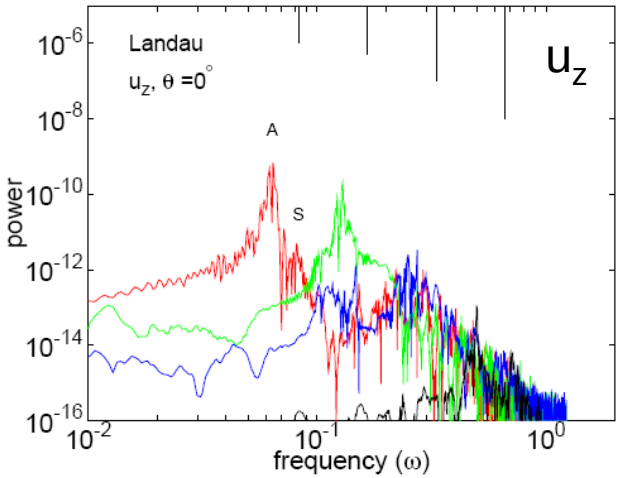

Sound waves are strongly damped

$k_x = 0, k_y = 0, k_z d_i = m/16$, where $m = 1$ (red), $m = 2$ (green), $m = 4$ (blue), $m = 8$ (black).

Hall-MHD FLR-Landau fluid

Slow (S) and fast (F) magnetosonic waves for the propagation angle of 45°

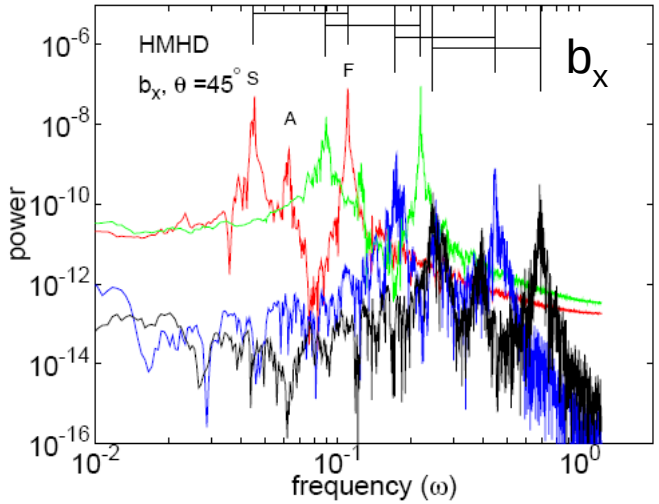

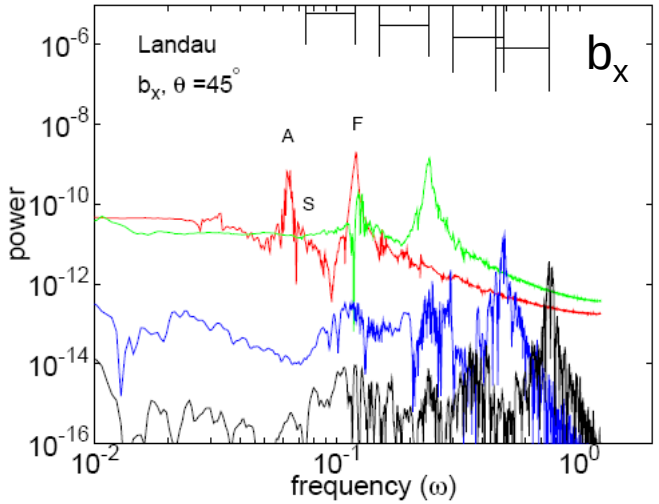

Slow waves are strongly damped

Alfvén waves for the propagation angle of 45°

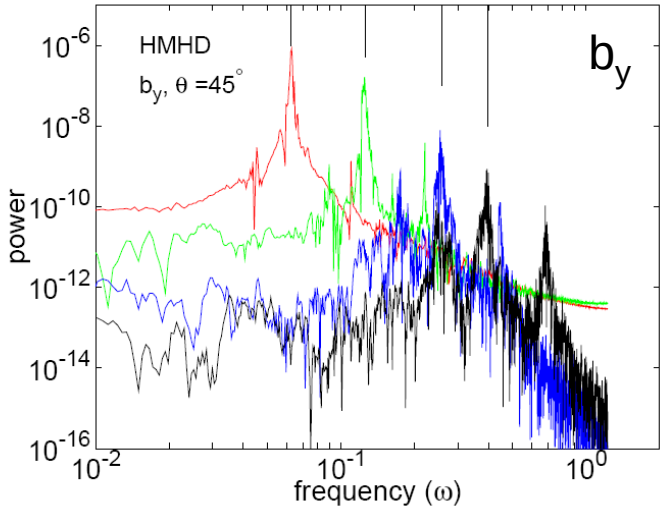

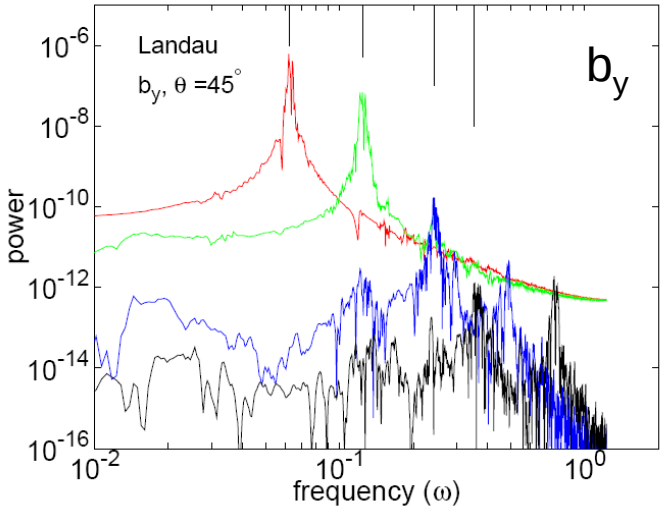

$k_y = 0, k_x d_i = k_z d_i = m/16$, where $m = 1$ (red), $m = 2$ (green), $m = 4$ (blue), $m = 6$ (black)

Hall-MHD

FLR-Landau fluid

Frequency shift due to FLR corrections

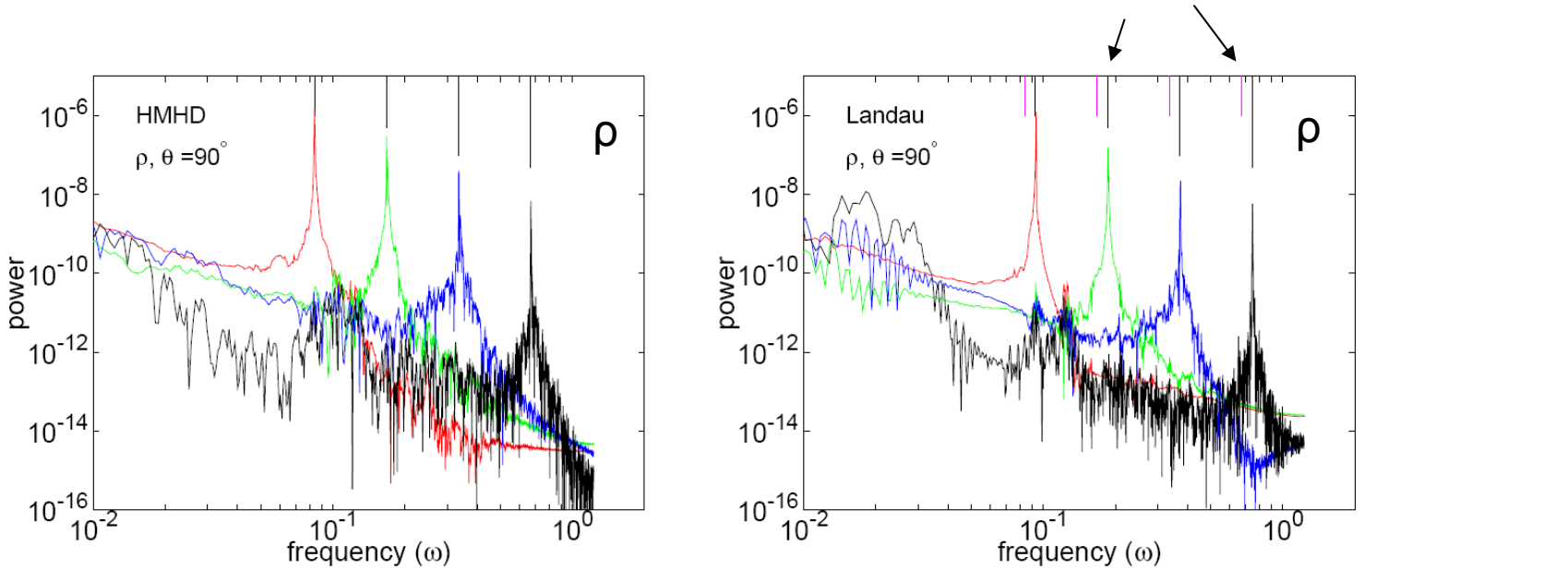

Magnetosonic waves for the propagation angle of 90°

frequency analysis of density modes with wavenumbers $k_y = 0, k_z = 0, k_x d_i = m/16$, where $m = 1$ (red), $m = 2$ (green), $m = 4$ (blue), $m = 8$ (black).

Spectral anisotropy

Hall-MHD

FLR-Landau fluid

Transverse directions

Parallel direction

Kinetic energy

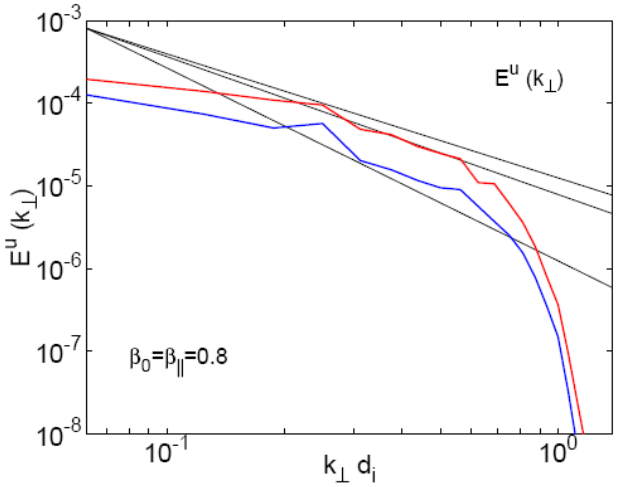

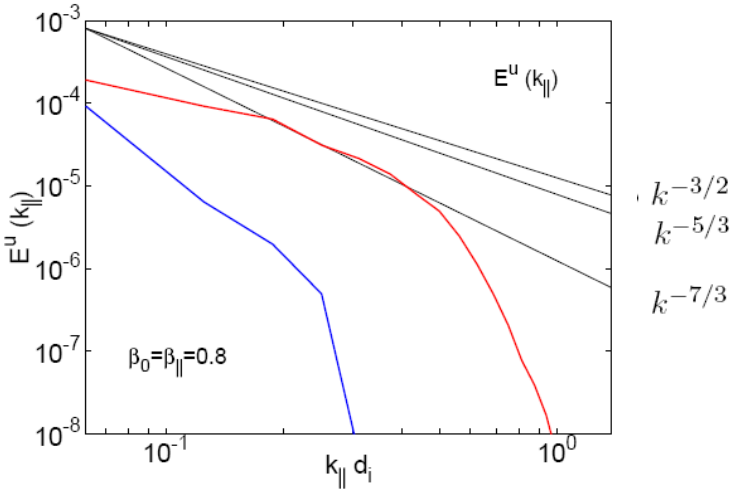

Magnetic energy

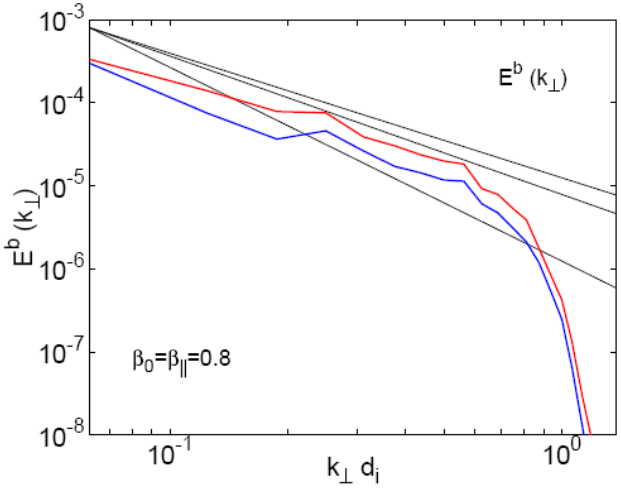

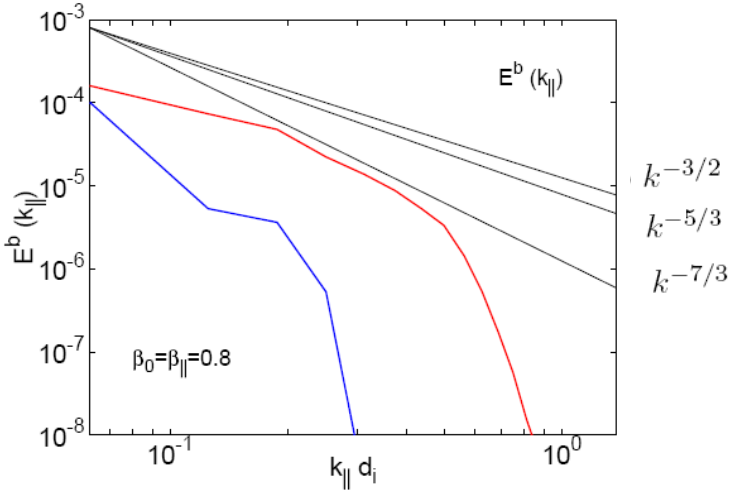

Strong reduction of the parallel transfer

Summary

FLR Landau fluids suitable for plasma dynamics at the ion gyroscale.

They retain

hydrodynamic nonlinearities + linear approximation of low-frequency kinetic effects (Landau damping & FLR corrections)

Consistent with the quasi-transverse character of the turbulent cascade.
Suitable for simulations of the solar wind.

Landau damping: depletes compressible effects and inhibits longitudinal transfer
leads to a correct description of the mirror instability.

FLR corrections: arrest of mirror instability at smal scales

A sufficiently accurate description of the FLR is needed to prevent small-scale spurious instabilities.

Suitable for addressing the problem of ion perpendicular heating (T. Passot's talk).